



Diffuse reflectance spectroscopy of human liver tumor specimens - towards a tissue differentiating optical biopsy needle using light emitting diodes

ALINA KELLER,^{1,*} PIOTR BIALECKI,¹ TORSTEN JOHANNES WILHELM,^{2,3} AND MARCUS KLAUS VETTER^{1,3}

¹Department of Embedded Systems and Biomedical Engineering, Hs Mannheim, University of Applied Sciences, 68163 Mannheim, Germany

²Department of Surgery, University Medical Center Mannheim, University of Heidelberg, 68167 Mannheim, Germany

³These authors contributed equally to this work

*a.keller@hs-mannheim.de

Abstract: Significant numbers of liver biopsies fail to yield representative tissue samples. This study was conducted to evaluate the ability of LED-based diffuse reflectance spectroscopy to discriminate tumors from liver parenchyma. Ex vivo spectra were acquired from malignant lesions and liver parenchyma of 32 patients who underwent liver resection using a white light source and several LEDs. Integrated spectra of two combined LEDs with emission peaks at 470 nm and 515 nm were classified with 98.4% sensitivity and 99.2% specificity. The promising results could yield to a simple handheld and cost-efficient tool for real-time tissue differentiation implemented in a biopsy needle.

© 2018 Optical Society of America

OCIS codes: (170.6935) Tissue characterization; (170.6510) Spectroscopy, tissue diagnostics; (230.3670) Light-emitting diodes; (060.2310) Fiber optics; (170.4580) Optical diagnostics for medicine; (170.1610) Clinical applications

References and links

1. A. Ananthakrishnan, V. Gogineni, and K. Saeian, "Epidemiology of Primary and Secondary Liver Cancers," *Semin. Intervent. Radiol.* **23**(1), 47–63 (2006).
2. S. M. Francque, F. F. De Pauw, G. H. Van den Steen, E. A. Van Marck, P. A. Pelckmans, and P. P. Michielsen, "Biopsy of focal liver lesions: guidelines, comparison of techniques and cost-analysis," *Acta Gastroenterol. Belg.* **66**(2), 160–165 (2003).
3. L. L. de Boer, B. H. W. Hendriks, F. van Duijnhoven, M. T. Peeters-Baas, K. Van de Vijver, C. E. Loo, K. Józwiak, H. J. C. M. Sterenberg, and T. J. M. Ruers, "Using DRS during breast conserving surgery: identifying robust optical parameters and influence of inter-patient variation," *Biomed. Opt. Express* **7**(12), 5188–5200 (2016).
4. D. J. Evers, R. Nachabé, M. J. Vranken Peeters, J. A. van der Hage, H. S. Oldenburg, E. J. Rutgers, G. W. Lucassen, B. H. Hendriks, J. Wesseling, and T. J. Ruers, "Diffuse reflectance spectroscopy: towards clinical application in breast cancer," *Breast Cancer Res. Treat.* **137**(1), 155–165 (2013).
5. R. Nachabé, D. J. Evers, B. H. Hendriks, G. W. Lucassen, M. van der Voort, E. J. Rutgers, M. J. Peeters, J. A. Van der Hage, H. S. Oldenburg, J. Wesseling, and T. J. Ruers, "Diagnosis of breast cancer using diffuse optical spectroscopy from 500 to 1600 nm: comparison of classification methods," *J. Biomed. Opt.* **16**(8), 087010 (2011).
6. J. Q. Brown, L. G. Wilke, J. Geradts, S. A. Kennedy, G. M. Palmer, and N. Ramanujam, "Quantitative optical spectroscopy: a robust tool for direct measurement of breast cancer vascular oxygenation and total hemoglobin content in vivo," *Cancer Res.* **69**(7), 2919–2926 (2009).
7. J. W. Spliethoff, L. L. de Boer, M. A. J. Meier, W. Prevoo, J. de Jong, T. M. Bydlon, H. J. C. M. Sterenberg, J. A. Burgers, B. H. W. Hendriks, and T. J. M. Ruers, "Spectral sensing for tissue diagnosis during lung biopsy procedures: The importance of an adequate internal reference and real-time feedback," *Lung Cancer* **98**, 62–68 (2016).
8. J. W. Spliethoff, D. J. Evers, H. M. Klomp, J. W. van Sandick, M. W. Wouters, R. Nachabé, G. W. Lucassen, B. H. Hendriks, J. Wesseling, and T. J. Ruers, "Improved identification of peripheral lung tumors by using diffuse reflectance and fluorescence spectroscopy," *Lung Cancer* **80**(2), 165–171 (2013).

9. D. J. Evers, R. Nachabé, H. M. Klomp, J. W. van Sandick, M. W. Wouters, G. W. Lucassen, B. H. Hendriks, J. Wesseling, and T. J. Ruers, "Diffuse reflectance spectroscopy: a new guidance tool for improvement of biopsy procedures in lung malignancies," *Clin. Lung Cancer* **13**(6), 424–431 (2012).
10. M. P. Bard, A. Amelink, M. Skurichina, V. Noordhoek Hegt, R. P. Duin, H. J. Sterenborg, H. C. Hoogsteden, and J. G. Aerts, "Optical spectroscopy for the classification of malignant lesions of the bronchial tree," *Chest* **129**(4), 995–1001 (2006).
11. W. C. Lin, D. I. Sandberg, S. Bhatia, M. Johnson, S. Oh, and J. Ragheb, "Diffuse reflectance spectroscopy for in vivo pediatric brain tumor detection," *J. Biomed. Opt.* **15**(6), 061709 (2010).
12. W. C. Lin, D. I. Sandberg, S. Bhatia, M. Johnson, G. Morrison, and J. Ragheb, "Optical spectroscopy for in-vitro differentiation of pediatric neoplastic and epileptogenic brain lesions," *J. Biomed. Opt.* **14**(1), 014028 (2009).
13. W. C. Lin, S. A. Toms, M. Johnson, E. D. Jansen, and A. Mahadevan-Jansen, "In vivo brain tumor demarcation using optical spectroscopy," *Photochem. Photobiol.* **73**(4), 396–402 (2001).
14. Y. Yu, C. Xiao, K. Chen, J. Zheng, J. Zhang, X. Zhao, and X. Xue, "Different optical properties between human hepatocellular carcinoma tissues and non-tumorous hepatic tissues in vitro," *J. Huazhong Univ. Sci. Technolog. Med. Sci.* **31**(4), 515–519 (2011).
15. E. Tanis, D. J. Evers, J. W. Spliethoff, V. V. Pully, K. Kuhlmann, F. van Coevorden, B. H. Hendriks, J. Sanders, W. Prevoo, and T. J. Ruers, "In vivo tumor identification of colorectal liver metastases with diffuse reflectance and fluorescence spectroscopy," *Lasers Surg. Med.* **48**(9), 820–827 (2016).
16. J. W. Spliethoff, L. L. de Boer, M. A. Meier, W. Prevoo, J. de Jong, K. Kuhlmann, T. M. Bydlon, H. J. Sterenborg, B. H. Hendriks, and T. J. M. Ruers, "In vivo characterization of colorectal metastases in human liver using diffuse reflectance spectroscopy: toward guidance in oncological procedures," *J. Biomed. Opt.* **21**(9), 97004 (2016).
17. D. J. Evers, R. Nachabé, D. Hompes, F. van Coevorden, G. W. Lucassen, B. H. Hendriks, M. L. van Velthuisen, J. Wesseling, and T. J. Ruers, "Optical sensing for tumor detection in the liver," *Eur. J. Surg. Oncol.* **39**(1), 68–75 (2013).
18. R. Nachabé, D. J. Evers, B. H. Hendriks, G. W. Lucassen, M. van der Voort, J. Wesseling, and T. J. Ruers, "Effect of bile absorption coefficients on the estimation of liver tissue optical properties and related implications in discriminating healthy and tumorous samples," *Biomed. Opt. Express* **2**(3), 600–614 (2011).
19. C. P. Hsu, M. K. Razavi, S. K. So, I. H. Parachikov, and D. A. Benaron, "Liver Tumor Gross Margin Identification and Ablation Monitoring during Liver Radiofrequency Treatment," *J. Vasc. Interv. Radiol.* **16**(11), 1473–1478 (2005).
20. R. Nachabé, B. H. Hendriks, R. Schierling, J. Hales, J. M. Racadio, S. Rottenberg, T. J. Ruers, D. Babic, and J. M. Racadio, "Real-time in vivo characterization of primary liver tumors with diffuse optical spectroscopy during percutaneous needle interventions. Feasibility study in woodchucks," *Invest. Radiol.* **50**(7), 443–448 (2015).
21. R. Priore, F. Trotta, G. Carlini, C. Zonta, A. Gaspari, C. Ferrari, M. Cova, and P. Dionigi, "A spectroscopy based procedure for in-vivo detection of liver metastasis in a rat model," *IJLM* **3**(2), 1–14 (2008).
22. A. Keller, P. Bialecki, and M. Vetter, "Comparison between total photon count and discrete spectral bands-normalization using DRS measurements for differentiation of tissues for liver biopsies," *Int. J. CARS* **10**(1), 32–33 (2015).
23. S. Pimenta, E. M. Castanheira, and G. Minas, "Optical microsystem for analysis of diffuse reflectance and fluorescence signals applied to early gastrointestinal cancer detection," *Sensors (Basel)* **15**(2), 3138–3153 (2015).
24. J. Y. Lo, B. Yu, H. L. Fu, J. E. Bender, G. M. Palmer, T. F. Kuech, and N. Ramanujam, "A strategy for quantitative spectral imaging of tissue absorption and scattering using light emitting diodes and photodiodes," *Opt. Express* **17**(3), 1372–1384 (2009).
25. A. Bogomolov, V. Ageev, U. Zabarylo, I. Usenov, F. Schulte, D. Kirsanov, V. Belikova, O. Minet, E. Feliksberger, I. Meshkovsky, and V. Artyushenko, "LED-based near infrared sensors for cancer diagnostics," *Proc. SPIE* **9715**, 971510 (2015).
26. T. M. Bydlon, R. Nachabé, N. Ramanujam, H. J. Sterenborg, and B. H. Hendriks, "Chromophore based analyses of steady-state diffuse reflectance spectroscopy: current status and perspectives for clinical adoption," *J. Biophotonics* **8**(1-2), 9–24 (2015).
27. Python Software Foundation, "Python Language Reference," version 2.7.13. <http://www.python.org>
28. F. Pedregosa, G. Varoquaux, A. Gramfort, V. Michel, B. Thirion, O. Grisel, M. Blondel, P. Prettenhofer, R. Weiss, V. Dubourg, J. Vanderplas, A. Passos, D. Cournapeau, M. Brucher, M. Perrot, and É. Duchesnay, "Scikit-learn: Machine Learning in Python," *JMLR* **12**, 2825–2830 (2011).
29. E. Jones, T. Oliphant, and P. Peterson, "SciPy: Open source scientific tools for Python," <http://www.scipy.org/>
30. G. C. Cawley and N. L. Talbot, "On Over-fitting in Model Selection and Subsequent Selection Bias in Performance Evaluation," *JMLR* **11**, 2079–2107 (2010).
31. R. Nachabé, B. H. Hendriks, M. van der Voort, A. E. Desjardins, and H. J. Sterenborg, "Estimation of biological chromophores using diffuse optical spectroscopy: benefit of extending the UV-VIS wavelength range to include 1000 to 1600 nm," *Biomed. Opt. Express* **1**(5), 1432–1442 (2010).
32. X. Chen, S. T. Cheung, S. So, S. T. Fan, C. Barry, J. Higgins, K. M. Lai, J. Ji, S. Dudoit, I. O. Ng, M. Van De Rijn, D. Botstein, and P. O. Brown, "Gene expression patterns in human liver cancers," *Mol. Biol. Cell* **13**(6), 1929–1939 (2002).

33. T. Kitai, M. Miwa, H. Liu, B. Beauvoit, B. Chance, and Y. Yamaoka, "Application of near-infrared time-resolved spectroscopy to rat liver--a preliminary report for surgical application," *Phys. Med. Biol.* **44**(8), 2049–2061 (1999).
34. C. T. Germer, A. Roggan, J. P. Ritz, C. Isbert, D. Albrecht, G. Müller, and H. J. Buhr, "Optical properties of native and coagulated human liver tissue and liver metastases in the near infrared range," *Lasers Surg. Med.* **23**(4), 194–203 (1998).

1. Introduction

Diagnosis and management of liver tumors play a significant role in modern cancer treatment. While hepatocellular carcinoma (HCC) is the 6th most frequent cause of cancer worldwide, approximately 40%-50% of extrahepatic malignancies spread to the liver [1]. Liver biopsy is a crucial component for initial diagnosis as well as molecular analysis during the course of treatment to define the best patient tailored treatment.

Some liver lesions are difficult to biopsy and repeated biopsies might be necessary, especially when lesions are small or poorly defined by ultrasound or computed tomography. Even with imaging guidance methods, up to 15% of liver biopsies are insufficient due to a sampling of non-informative tissues [2]. Such failures are caused by a lack of recognition of tumor tissue during biopsy, which results in a repetition of the biopsy thus increasing the risk of hemorrhage and possibly needle tract seeding. In combination with the standard imaging techniques the integration of an *in vivo* tissue differentiation device in the tip of a common biopsy needle yields an additional source of local information which can potentially achieve a higher biopsy success rate.

Diffuse reflectance spectroscopy (DRS) is a highly promising technique for tissue recognition during biopsy. Several studies demonstrate the feasibility of DRS to differentiate tumors from unaffected parenchyma in different organ systems such as breast [3–6], lung [7–10] and brain [11–13] both *ex vivo* and *in vivo*. The non-invasive optical measurement technique utilizes light absorption and scattering after its interaction with cells and molecules. These light-tissue interactions are used to extract information about the underlying biochemical composition and morphological structure of the analyzed tissue.

Spectroscopic detection of malignant tumors in liver specimens has been successfully performed for primary liver cancer [14] and liver metastases in humans [15–19] as well as in animal models [20,21]. In a clinical *ex vivo* study by Evers et al. [17] liver specimen of 24 patients who underwent surgery for colorectal liver metastases were analyzed with DRS in the visible (VIS) and near infrared (NIR) spectral range. DRS achieved a sensitivity and specificity of 94% in discriminating liver metastases from unaffected liver parenchyma. The authors were able to estimate various chromophore volume fractions. Total hemoglobin, fat and bile content turned out to be most discriminative parameters for tissue differentiation. Yu et al. [14] obtained optical properties from 38 *ex vivo* human liver tissues with HCC. Using the VIS wavelength range, absorption and scattering coefficients were significantly different between non- and tumorous tissue mainly between 400 nm and 500 nm. Furthermore, a recently published study by Tanis et al. [15] demonstrated that DRS can accurately discriminate colorectal liver metastases from liver parenchyma in the *in vivo* setting. Liver tissue of 19 liver tumor patients were analyzed prior to resection and classified with an overall sensitivity and specificity of 95% and 92%, respectively. Similarly, to the above mentioned *ex vivo* studies, bile was found to be the most significantly discriminative tissue chromophore for *in vivo* tumor detection in the liver.

The major benefit of DRS is its ability to perform non-invasive tissue characterization in near real-time without the need for exogenous contrast agents. In most of the studies mentioned above, the measurement setups consist of expensive and complex spectroscopic systems (i.e. broadband light source, fiber optic probe, and spectrometer). In order to proceed to further clinical utilization the optical needle needs to fulfill the requirement for a compact, cost-effective, and hand-held tool for biopsy. By replacing the light source and the spectrometer with high power light emitting diodes (LEDs) and photodiodes, a major step

towards a miniaturized and inexpensive assistance tool for biopsy with high clinical utility could be achieved.

Several groups have recently concentrated on the progress of tissue differentiating methods using only a few, but representative, spectral bands in DRS [22–25]. The results suggest that this simplification is not necessarily associated with a loss in classification accuracy. We have demonstrated that classification accuracy of diffuse reflectance measurements of different animal tissues (liver and fat) using several selected spectral ranges delivers comparable results to the analysis of the entire broadband spectrum [22]. Therefore, an *in vivo* tissue differentiation can potentially be achieved by using LEDs for tissue illumination and photodiodes for detection of the reflected light.

This is the first study to examine the use of LEDs in the VIS and NIR spectrum for tissue differentiation in the liver. The potential of LED-based DRS was investigated *ex vivo* on liver specimens with malignant lesions from 32 patients undergoing liver resection. We present the ability of selected LEDs in comparison with DRS using a white light source (WS-based DRS) in order to discriminate liver parenchyma from tumorous tissue.

2. Materials and methods

Clinical study design

This study was conducted in collaboration with the Department of Surgery of the University Medical Center Mannheim between 2015 and 2017 under approval of the internal review board (2014-590N-MA). 32 adult patients undergoing liver resection for various primary or secondary liver tumors agreed to participate. Written consent was obtained from each patient before surgery. Exclusion criteria were HIV or hepatitis C infection, age below 18 years and parenchyma or tumor samples less than 1 cm in diameter. The aim was to evaluate the feasibility of LED-based DRS to differentiate tumorous and non-tumorous liver tissue.

Instrumentation

Ex vivo diffuse reflectance spectra were acquired using a portable spectroscopic system. The measurement concept consisted of several selective light sources based on LED as well as a baseline system providing a continuous broadband spectrum. Spectral recording was achieved using a portable spectrometer (USB4000-VIS-NIR-ES, Ocean Optics) with a 3648-element charge-coupled device array detector covering a wavelength range from 344 nm to 1044 nm. The fiberoptic reflectance probe (QR400-7-VIS-NIR, Ocean Optics), used in both measurement setups, consisted of seven 400 μm core-diameter optical fibers within a six-around-one fiber bundle design. A control software, programmed using MATLAB (Version R2017a, Mathworks, Massachusetts, USA), was used to operate the spectrometer and to store the acquired measurement data.

For selective light source measurements ten different high power LEDs (Roithner Lasertechnik GmbH, Vienna, Austria) were positioned on a round mount connected via a shaft to a mechanical selector switch. Each LED was powered by a separate constant current source to ensure stable brightness. An optical diffuser (CC-3, Ocean Optics) collected light from 180° field of view and coupled it into the multi-fiber bundle. The single fiber was connected to the spectrometer. The entire construction was shielded from ambient light.

The selection of used LEDs was based on publications by Nachabé et al. [18] and Bydlon et al. [26]. They summarized wavelength-dependent absorption characteristics of various chromophores with their relevance for the liver and effect on optical properties after tumorous changes. In liver tissue diffuse reflectance spectra in the VIS and NIR wavelength range are mainly influenced by two main blood chromophores (deoxygenated and oxygenated hemoglobin), bile, water, and lipids. LED01 was chosen because of the chromophore bile with its main absorption peak at 409 nm, whereas LED02 and LED03 were chosen to be close

to the absorption peaks of oxygenated and deoxygenated hemoglobin. The maximal peak wavelengths of LED04 to LED10 mostly corresponded to the absorption of water and lipids.

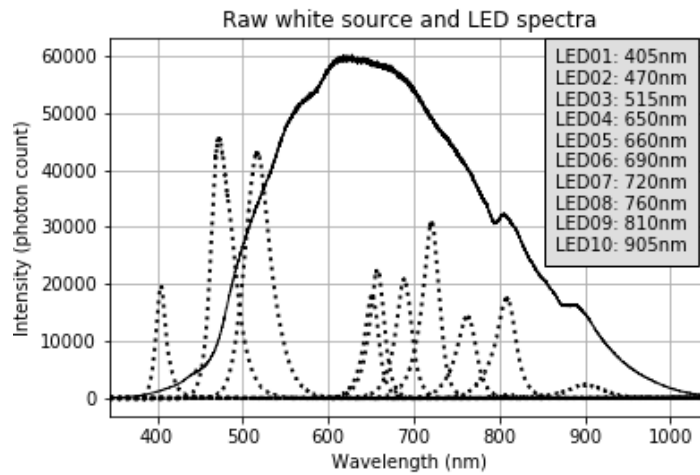


Fig. 1. Reflectance spectra of white light source (solid line, integration time 45 ms) and ten different high power LEDs (dashed lines, integration time 100 ms) measured with a reflectance standard.

For the baseline measurements a Tungsten halogen light (HL-2000, Ocean Optics, Dunedin, Florida) provided light emission in the VIS and NIR spectral range (360 nm to 2400 nm). In this WS-based setup the single fiber delivered light to the tissue, while the remaining external fibers collected diffuse reflectance from the tissue sample to the spectrometer. Figure 1 illustrates the spectral output of the WS (solid line) as well as of the ten different high power LEDs (dashed lines) numbered consecutively from left to right in the given setup.

Optical measurements

Prior to each experiment, both spectroscopic setups (WS-based and LED-based) were adjusted using a diffuse reflectance standard (WS-1, Ocean Optics) to ensure the consistency of white light and LED power as well as other instrumental parameters. A dark spectrum (i.e. no excitation and ambient light) was captured to correct the measurement spectra for instrument response variables. Immediately after resection, the surgeon made incisions through liver parenchyma and liver tumors. Measurement sites were defined with different colored markers evenly distributed over the lesion and liver parenchyma, exemplarily shown in Fig. 2. All tumors included had a macroscopically homogenous cut surface. There were no tumors with a visible central tumor necrosis. The total number of investigated sites in each patient varied from two to five in liver parenchyma and from two to eight in tumorous tissue, depending on the specimen size. The average time span from tissue resection to the beginning of the LED-based DRS was 14 ± 8 minutes. After lightly dabbing the sample surface with a tissue paper to remove any residual blood, the fiberoptic probe was placed in direct contact with the tissue sample. Probe contact pressure was maintained at a level for which tissue deformation was not visible.

At first, diffuse reflectance spectra were acquired with LED-based DRS (average measurement time 17 ± 7 minutes). For each measuring point DRS spectra were successively captured using 10 LEDs. Per LED a total of 10 spectra was recorded. This procedure was repeated for all following measurement sites. Then measurements were performed with WS-based DRS (average measurement time 6 ± 2 minutes) following the before-mentioned procedure, i.e. recording 10 spectra per measuring site. During spectral data acquisition, the overhead lighting was temporarily turned off to minimize the contribution of ambient light to

the optical spectra. All measurement sites where the probe was visibly covered in blood were marked as invalid in the standard protocol and excluded from further processing. At the end of each measurement, the specimen was returned to the operating room, formalin-fixed and routinely passed on to histopathology for further investigation.

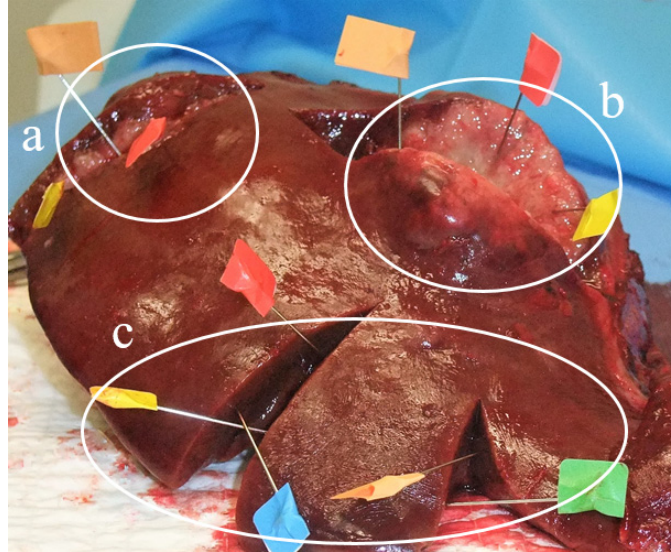


Fig. 2. Representative example of a resected liver with two malign lesions which are metastases from rectal cancer. The colored markers in a and b describe the 6 measurement sites on tumorous tissue. The remaining measurement sites in c are defined on liver parenchyma.

Data processing and analysis

Before any analysis was conducted, reflectance spectra were processed to remove instrument-introduced variations in both, measurements with WS and LEDs using MATLAB. For each measurement site that was investigated, the mean spectrum was calculated from its corresponding spectral data set. This procedure might eliminate artefacts in the measurement data introduced by involuntarily hand movements during the data recording. A baseline correction was performed, by subtracting the dark spectrum from each corresponding measurement spectrum. To eliminate inter-patient variations in reflectance spectra of WS-based DRS, the data was normalized. For this purpose, each continuous spectrum was divided by its maximum intensity value, thus scaling the intensities of each signal between zero and one. For reflectance spectra of the ten different LEDs the total photon count was calculated, by summing over each measurement spectrum separately, resulting in one scalar value per LED per measurement site.

In accordance with their histopathological identities, all measurements were divided into two categories: liver parenchyma and tumorous tissue. We used several scientific python libraries and tools to analyze the present measurements [27–29]. Since no assumption about the classification model and its hyper-parameters could be made, a nested cross-validation (CV) scheme was implemented. The nested CV consists of an outer CV for model selection and an inner CV for hyper parameter tuning of the current model. Utilizing this procedure, an overly-optimistic score of the classifier will be prevented [30].

Since we assume that the measurements of one patient are correlated, both the inner and outer CV loops were implemented as a Leave-One-Patient-Out CV, where for each CV split all measurements of one patient were removed from training and used for validation.

In the outer CV loop, a linear discriminant analysis (LDA) was performed on the training set of WS reflectance spectra to reduce the dimensionality of the data set to ten linear components. No dimensionality reduction was necessary for LED-based DRS. Support

Vector Machines (SVMs) were tuned in the inner CV loop and used for classification of the data set in the outer CV loop. For the WS-based DRS measurements all ten linear components provided by LDA were used as features for classification. To keep the measurement system as compact as possible, we used measurements from single as well as combinations of two LEDs for LED-based DRS to train the classifier. For each run, the pipeline returned the predictions for the current hold-out test patient. These predictions were compared to the reference information of the measurement site (ground truth) and used to evaluate sensitivity and specificity of the classification pipeline.

3. Results

During the study period of 21 months, liver specimens were collected from 32 liver tumor patients with a mean age of 66 ± 11.5 (range 39-84) years. The patient population consists of 20 males (62.5%) and 12 females (37.5%). Of the 32 patients nine had primary tumors and 23 secondary tumors (Table 1). Primary tumors were HCC or cholangiocellular carcinomas (CCC). Secondary tumors were predominantly metastases from colorectal cancer. The mean time between resection and beginning of the measurement was 14 ± 8 minutes with LED-based DRS and 28 ± 23 minutes with WS-based DRS. Of the 32 patients 13 (40.6%) had a history of receiving chemotherapy.

Table 1. Specification of liver tumors

	Tumor type	Number of patients
Primary tumor	HCC	7
	CCC	2
Secondary tumor	Rectal	10
	Colon	7
	GIST ^a	3
	Others ^b	3

^agastrointestinal stromal tumors; ^bchronic lymphoid leukemia, lung carcinoid tumor, renal cell carcinoma

In total, 123 measurements on liver parenchyma sites and 131 measurements on tumorous sites were performed. Because of blood contamination at the probe tip during the examination, one measurement of liver parenchyma and three measurements of tumorous tissue have been excluded from the statistical analysis of WS-based DRS. LED-based data of the first patient has been excluded, because of defects in the measurement setup as well as one further measurement site on liver tissue because of blood contamination at the tip of the probe.

Figure 3 illustrates the average WS reflectance spectra of liver (solid line) and tumor (dashed line) after baseline correction (top) and additionally with normalization (bottom). The standard deviation of each type of tissue is represented as hatched and grey areas for liver parenchyma and tumor, respectively.

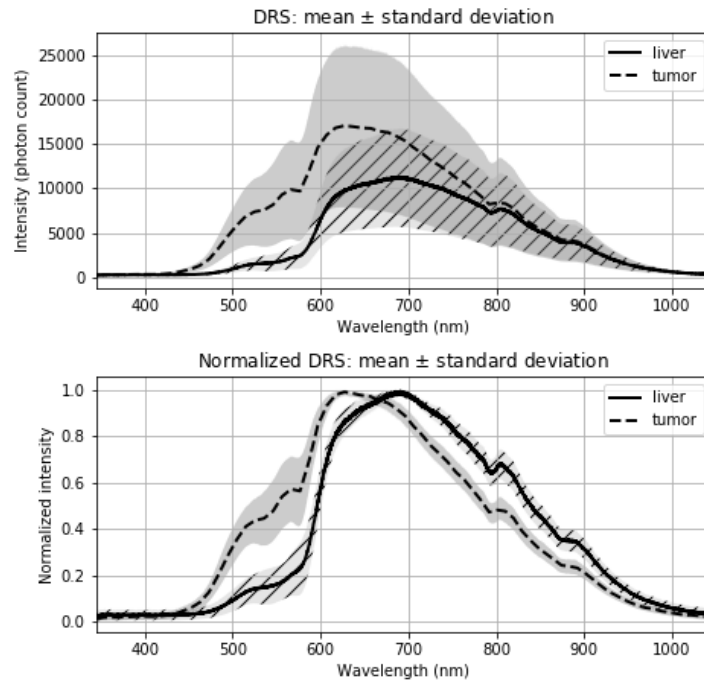


Fig. 3. Mean diffuse reflectance spectra of liver parenchyma (solid line) and tumorous tissue (dashed line) using a broadband light source in the VIS and NIR spectral range before (top) and after (bottom) normalization. The hatched (liver parenchyma) and grey (tumor) areas indicate the standard deviation of each type of tissue.

Almost over the entire spectrum, the mean reflected intensity of malignant tissue is higher compared to the mean intensity from liver parenchyma, displayed in Fig. 3 (top). The mean spectrum of liver parenchyma shows high absorption of light between 450 nm to nearly 600 nm, resulting in a small positive slope, whereas the mean intensity of tumorous tissues increases up to its maximum at 620 nm. The maximum mean intensity of the DRS from liver parenchyma is located around 700 nm. In addition, the standard deviation of diffuse reflectance spectra from tumorous tissue (grey area) is larger than from liver parenchyma (hashed area) mainly at 500 nm to 800 nm. Considering the entire reflectance spectrum of liver tissue measurements, the intra- and inter-patient variation between 500 nm and 600 nm is very low.

Because of inter-patient variance, all spectra were normalized by their maximum intensities. Figure 3 (bottom) shows the WS reflectance spectra after the normalization. As can be seen, the normalization reduces the variance in the spectra while the spectral shape remains unchanged. The results of the analysis are presented in Table 2. For each patient the ratio of the number of correctly classified tissue measurements for both liver parenchyma and malignant liver lesions is illustrated. The classification of the types of tissue is based on the diffuse reflectance spectra without normalization as well as with normalization. The predictions of the data without normalization shows a sensitivity and specificity of 90.6% and 93.4%, respectively, with an overall accuracy of 92%. After normalization of the measurement data, the classification accuracy has been improved to 98.4% with only two misclassified measurements per type of tissue, from both, tissue samples of patient with primary and secondary liver tumors (sensitivity = 98.4% and specificity = 98.6%).

Table 2. Per patient classification based on SVM with Leave-One-Patient-Out CV of DRS with selected LED combination, white source and normalized white source measurements.

Patient number	LED2 vs LED3		WS		normalized WS	
	Liver	Tumor	Liver	Tumor	Liver	Tumor
1	NA	NA	(5/5)	(6/6)	(5/5)	(6/6)
2	(4/4)	(3/3)	(3/3)	(1/3)	(3/3)	(3/3)
3	(5/5)	(6/6)	(5/5)	(6/6)	(5/5)	(6/6)
4	(5/5)	(5/5)	(5/5)	(4/5)	(5/5)	(5/5)
5	(5/5)	(8/8)	(4/5)	(8/8)	(4/5)	(8/8)
6	(3/3)	(2/2)	(2/3)	(2/2)	(3/3)	(2/2)
7	(5/5)	(5/5)	(5/5)	(5/5)	(5/5)	(5/5)
8	(4/4)	(5/5)	(5/5)	(2/5)	(5/5)	(5/5)
9	(5/5)	(5/5)	(5/5)	(5/5)	(5/5)	(5/5)
10	(5/5)	(5/5)	(4/5)	(5/5)	(5/5)	(5/5)
11	(5/5)	(5/5)	(3/5)	(5/5)	(5/5)	(5/5)
12	(5/5)	(6/6)	(4/5)	(6/6)	(5/5)	(6/6)
13	(3/3)	(3/3)	(3/3)	(3/3)	(3/3)	(3/3)
14	(3/3)	(3/3)	(3/3)	(3/3)	(3/3)	(3/3)
15	(3/3)	(4/4)	(2/3)	(4/4)	(3/3)	(4/4)
16	(5/5)	(5/5)	(5/5)	(5/5)	(5/5)	(5/5)
17	(3/3)	(2/2)	(3/3)	(2/2)	(3/3)	(2/2)
18	(5/5)	(5/5)	(5/5)	(5/5)	(5/5)	(5/5)
19	(5/5)	(5/5)	(5/5)	(2/5)	(5/5)	(5/5)
20	(2/2)	(3/3)	(2/2)	(3/3)	(2/2)	(3/3)
21	(2/2)	(2/2)	(2/2)	(2/2)	(2/2)	(2/2)
22	(2/2)	(3/3)	(2/2)	(2/2)	(2/2)	(2/2)
23	(3/3)	(3/3)	(3/3)	(3/3)	(3/3)	(3/3)
24	(3/3)	(5/5)	(3/3)	(3/3)	(3/3)	(3/3)
25	(4/4)	(4/4)	(4/4)	(4/4)	(4/4)	(4/4)
26	(3/3)	(3/3)	(3/3)	(3/3)	(3/3)	(3/3)
27	(5/5)	(5/5)	(5/5)	(3/5)	(5/5)	(4/5)
28	(2/3)	(3/3)	(3/3)	(3/3)	(2/3)	(3/3)
29	(3/3)	(3/3)	(3/3)	(3/3)	(3/3)	(3/3)
30	(2/2)	(2/2)	(2/2)	(2/2)	(2/2)	(2/2)
31	(5/5)	(5/5)	(5/5)	(5/5)	(5/5)	(5/5)
32	(2/2)	(0/2)	(1/2)	(1/2)	(2/2)	(1/2)
Correct	116	123	114	116	120	126
Total	117	125	122	128	122	128
Sensitivity	98.40		90.63		98.44	
Specificity	99.15		93.44		98.63	
Accuracy	98.76		92.00		98.40	

The measurement spectra of LED-based DRS have been integrated to one value per LED per measurement site. Figure 4 displays the classification accuracy of the summed reflectance spectra of the different LEDs separately, listed along the diagonal of the matrix, as well as in paired combinations. It can be seen that the best results arise from LED02 and LED03 in combination, with its maximum peak wavelengths at 470 nm and 515 nm, respectively. The single use of LED02 already achieves a classification accuracy of 97.9% and in combination with the reflectance spectra of LED03 an improved accuracy of 98.8%. As can be observed in the Scatterplot (Fig. 5), one measurement of liver tissue is predicted incorrectly as tumorous tissue and two measurement sites of malignant tissue were misclassified as liver parenchyma,

which yields a sensitivity of 98.4% and a specificity of 99.2% as presented in Table 2. The incorrectly classified measurements were derived from liver specimens of a metastasis of rectal carcinoma (patient 28) and one HCC (patient 32).

Mean Leave-One-Patient-Out CV accuracy of SVM

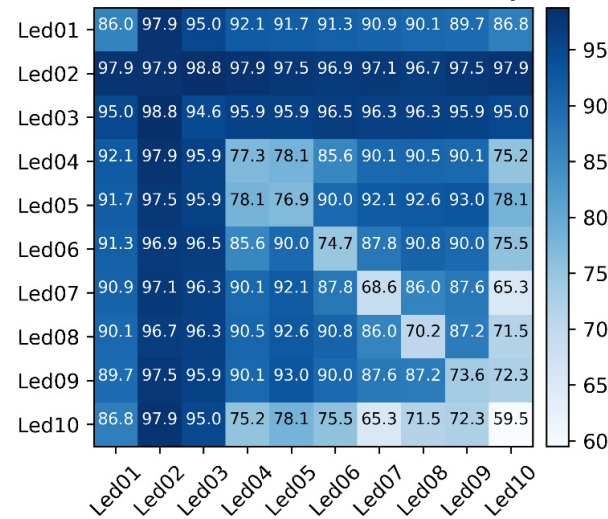


Fig. 4. Classification accuracy obtained from Leave-One-Patient-Out CV procedure based on SVM using integrated diffuse reflectance spectra of single LEDs and paired LED combinations.

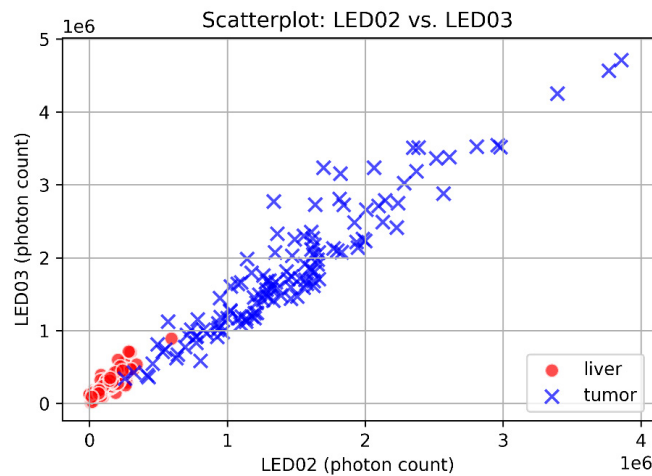


Fig. 5. Scatterplot of integrated photon counts from LED02 and LED03 of liver tissue (red spots) and malignant lesions (blue crosses).

The receiver operating characteristic curve (ROC curve) depicts the false positive rate in relation to the sensitivity for different probability thresholds for the best SVM classifier. Figure 6 shows the ROC curve for the classification of the summed spectral intensities of LED02 and LED03. The threshold for the desired classifier characteristic can be chosen by selecting a point on the ROC curve.

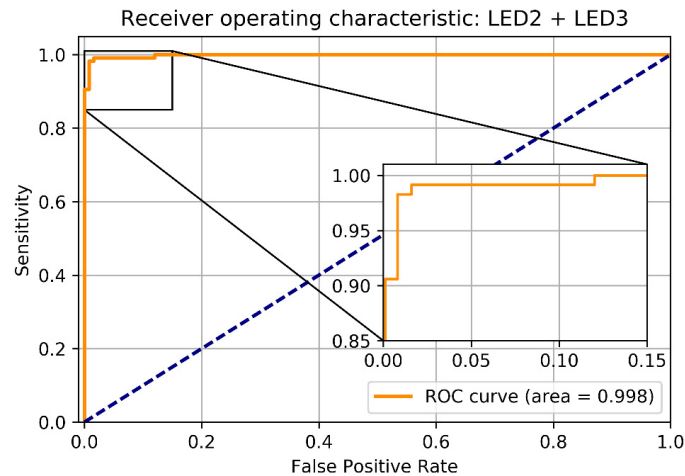


Fig. 6. Receiver operating characteristic curve of discriminating results based on integrated reflectance spectra values of LED02 and LED03. area: area under ROC curve

4. Discussion

In the present ex vivo study diffuse reflectance spectra were acquired from liver parenchyma and malignancies of 32 patients. Differences can be observed between diffuse reflectance spectra of the two examined types of tissue. Using a broadband light source, DRS can accurately discriminate liver parenchyma from malignant lesions with a sensitivity and specificity of 90.6% and 93.4%, respectively. Due to a high inter-patient variability and especially the heterogeneity of tumorous tissue, we performed a normalization with maximum intensity, which improved classification accuracy to 98.4% with a sensitivity of 98.4% and a specificity of 98.6%, respectively. The mean spectral measurements shown in Fig. 3 suggest that the optical properties of tissue types contain the most discriminative information for tissue classification in the VIS wavelength range between 450 nm and 750 nm. These findings are similar to those that have been reported for different ex vivo studies on human liver tissue of tumor patients with primary cancer [14], as well as with liver metastases [17–19].

In the present study we aimed to make the next crucial step towards clinical application of the promising DRS for tissue differentiation by performing LED-based DRS. We identified several emission wavelengths of LEDs where diffuse reflectance intensities from normal liver differ from those of malignancies. LEDs illuminating in the VIS spectral range, especially LED01 (405 nm), LED02 (470 nm), LED03 (515 nm) and LED04 (650 nm) achieved a classification accuracy between 77.3% and 97.9%. By determining the best LED combination (LED02 and LED03), accuracy was improved to 98.8% with a sensitivity and specificity of 98.4% and 99.2%, respectively. Misclassified measurements occurred in both DRS setups from liver samples of patients with primary, as well as with secondary tumors. The ROC curve (Fig. 6) can be used for adjusting the threshold values for a low false positive rate or a high sensitivity. In the case of a tissue differentiating biopsy needle a low false positive rate is clinically more desirable. Liver tissue would not be misclassified as tumorous tissue at the cost of a misclassification of tumor tissue. This means in a tissue classification algorithm, the diagnostic decision making would be advisable for a false positive rate near zero.

Each biological matter in an examined tissue sample has its intrinsic wavelength dependent optical absorption characteristic. As mentioned before, changes between types of tissue mainly occur in the VIS wavelength range caused by different compositions of light

absorbing chromophores. Important chromophores in the liver, absorbing in the wavelength range of LED01-LED04, are bile as well as oxygenated and deoxygenated hemoglobin [26].

In comparison with the diffuse reflectance spectra, it was noticed that the diffuse reflectance intensities from healthy tissue between 400 nm - 600 nm consistently were lower than those from tumor, displayed in Fig. 3 and Fig. 5. These observations originate from different chromophores for both primary and secondary tumor types. Since metastases consist of abnormal cells with their origin in other organs, the amount of bile with high absorption between 400 nm and 500 nm is low [17,18,31]. Extracted from diffuse reflectance spectra, Nachabé et al. [18] have shown that the amount of bile in metastatic tumor tissues is 80% lower than in healthy liver tissue. Although, primary liver cancer cells can produce bile, the diffuse reflectance spectra show comparable results of absorption in the wavelength range between 400 nm and 500 nm with spectra of metastases [14]. Yu et al. explain this finding with the presence of an additional chromophore existing mainly in the liver parenchyma called cytochrome P-450 [14]. This chromophore has its main absorption peak at 450 nm and its presence is relatively lower in primary liver cancer [32].

In addition, various studies have observed statistical differences in the oxygen saturation of blood between liver tissue and tumors [17,18,20]. Since we performed an ex vivo study, caution needs to be taken with regard to changes in oxygenation level after resection due to elimination of liver perfusion. Based on the study by Kitai et al. [33] we assume that measured hemoglobin oxygenation does not reflect the actual oxygenation level as it would do in vivo. However, tumors are known to have a vascular network of higher density than most normal tissues. Considering liver tissue, the opposite seems more likely, because it is characterized by a dense capillary network. Besides bile, the high absorption in the VIS wavelength range in liver tissue can be caused by the blood volume fraction, which is proven to be higher in healthy liver tissue [15,17,18,20,34].

Although our results are promising and we assume that a tumor sensing biopsy needle using LED-based DRS seems feasible in liver tissue, several shortcomings of our study have to be mentioned. First, various tissue parameters, for example tissue oxygenation, might significantly change after the specimen has been removed from the patient's body. However, we expect, that the most discriminative chromophores absorbing around 400 nm and 500 nm are unlikely to change significantly after resection. Nachabé et al. [20] presented the first in vivo real-time optical tissue characterization in woodchucks during percutaneous intervention using NIR DRS sensing at the tip of a needle. The measurements showed significant differences when the needle tip was moved from healthy liver tissue to primary liver cancer, mainly because of tissue blood volume fraction and oxygenation. Additionally, Tanis et al. [15] performed in vivo spectral data acquisition with DRS incorporated at the tip of a needle to discriminate colorectal liver metastases from normal liver tissue in 19 patients. Overall sensitivity and specificity were 95% and 92%, respectively, where bile was the most discriminative parameter. As our measurements were performed in comparable emission wavelengths, we assume that our ex vivo findings can be applied to an in vivo setting, which has to be verified in further studies. Second, the presence of blood around the needle tip cannot be disregarded due to needle feed in vivo. As total hemoglobin fraction is known to be one of the main discriminative absorbing parameter in the emission wavelength range of LED02 and LED03, the effect on optical measurements of local hemorrhage in the in vivo setting has to be investigated further. Third, we did not histologically examine each measurement site separately to confirm that the needle was positioned in tumor tissue. However, the macroscopic difference between the type of tissue was so distinct that misinterpretation seems extremely unlikely.

5. Conclusion

To our best knowledge, this is the first study that sought to assess the feasibility of LEDs as light sources for DRS to differentiate normal liver parenchyma and malignant liver lesions. In

sum, using DRS with a combination of two LEDs with maximal peak wavelength at 470 nm and 515 nm for tissue illumination, this method has successfully classified these types of tissue *ex vivo*. This advantage could yield to a simple handheld and cost-efficient tool for real-time tissue differentiation implemented in the tip of a biopsy needle. Providing crucial information about the tissue at the needle tip position before a tissue sample is taken may help to decrease the biopsy failure rate hence reduce biopsy procedure time, expense and patient's risk. With this compact device no further components need to be installed in the sterile field with minimal impact on clinical workflow. These expectations need to be confirmed in future *ex vivo* and *in vivo* studies.

For the future work a new prototype with the determined LEDs as well as photodiodes implemented in the biopsy needle tip is currently being developed. The prototype enables continuous measurements during needle insertion, thus allowing the co-registration between measurement data and its histologic examination at multiple sites of the branch canal, including determination of e.g. histologic fibrosis and necrosis degree.

Funding

German Federal Ministry of Education and Research (BMBF) within the Framework "Forschungscampus: public-private partnership for Innovations" (13GW0090A).

Acknowledgments

We would like to thank Volker Wunsch und Benjamin Glass for their involvement in the development of the measurement setup and Carla Gil and Benjamin Kraus for their support on data processing with helpful discussions.

Disclosure

The authors declare that there are no conflicts of interest related to this article.